Magnetism and magnetotransport in disordered graphene

T. G. Rappoport,[1] Bruno Uchoa,[2] and A. H. Castro Neto[3]

[1]*Instituto de Física, Universidade Federal do Rio de Janeiro, Rio de Janeiro 68.528-970, RJ, Brazil*
[2]*Department of Physics, University of Illinois at Urbana–Champaign, 1110 West Green Street, Urbana, Illinois 61801-3080, USA*
[3]*Department of Physics, Boston University, 590 Commonwealth Avenue, Boston, Massachusetts 02215, USA*

We perform Monte Carlo simulations to study the interplay of structural and magnetic order in single layer graphene covered with magnetic adatoms. We propose that the presence of ripples in the graphene structure can lead to clustering of the adatoms and to a variety of magnetic states such as superparamagnetism, antiferromagnetism, ferromagnetism and spin-glass behavior. We derive the magnetization hysteresis and also the magnetoresistance curves in the variable range hopping regime, which can provide experimental signatures for ripple induced clustering and magnetism. We propose that the magnetic states in graphene can be controlled by gate voltage and coverage fraction.

I. INTRODUCTION

Graphene is probably one of the most remarkable discoveries in condensed-matter physics in the last decade.[1,2] The material is a two-dimensional (2D) crystal composed of carbon (C) atoms with sp^2 hybridization; that is, graphene is one atom thick and thus the thinnest cloth in nature. Because of its low dimensionality, it does not show structural long-range order in its free form, as per the Hohenberg-Mermin-Wagner (HMW) theorem,[3] but it can present a flat phase at low temperatures due to nonlinear effects or in the presence of a substrate, scaffolds, contacts, or impurities that break explicitly the translational symmetry perpendicular to the graphene plane.[4] The leftovers of the fluctuations that forbid long-range order are found in the form of frozen ripples in suspended[5,6] samples.

While it was theoretically predicted early on that graphene by itself would not be magnetic,[7] it has been shown that adatoms in the graphene surface can easily form magnetic moments due to graphene's unusual electronic properties such as low density of states and chirality.[8] Moreover, because graphene has a low density of states close to the Dirac point, the Kondo effect is suppressed,[9,10] allowing for the appearance of magnetic states. On the other hand, because of its low dimensionality, long-range magnetic order is inhibited, and the intrinsic coupling between structural and magnetic fluctuations may lead to very inhomogeneous spin textures (such as of Griffiths phases[11]) that can be found in complex itinerant magnetic systems such as disordered Kondo Lattices.[12]

In this paper, performing a series of Monte Carlo simulations over disordered realizations of magnetic adatoms in a graphene sheet, we examine the magnetic correlations of the local moments in the magnetization and in the magnetoresistance curves. In the case of adatoms such as hydrogen (H), where the probability of adsorption changes substantially according to the local curvature of the graphene sheet, we show that the formation of local magnetic moments leads to an interesting interplay between the correlation due to the Ruderman-Kittel-Kasuya-Yosida (RKKY) interaction and the ripples, generating a variety of magnetic textures, ten-

dency to clustering at low concentrations and a percolative transition at higher concentration of adatoms. Since the overall magnetic response of a single layer is rather small compared to the usual response in bulk, magnetotransport measurements are probably the easiest way to probe magnetic correlations in graphene. Based in our Monte Carlo results for the magnetization, we calculate the magnetoresistance curves in graphene for strong disorder. These curves can offer clear experimental signatures for the presence of macroscopic magnetic states in graphene in the regime of variable range hopping.[13]

The structure of the paper is as follows: in Sec. II we introduce the spin Hamiltonian for the magnetic adatoms; in Sec. III we derive the heuristic rules for adsorption of adatoms in graphene, comparing different realizations of disorder for different adsorption probability distributions, which we define in terms of the curvature (height) of the ripples. In Sec. IV, we derive the magnetization curves and in Sec. V we calculate the magnetoresistance. Finally, in Sec. VI we present our conclusions.

II. RKKY HAMILTONIAN

Our starting point is the tight-binding Hamiltonian of the electrons in graphene (we set $\hbar = 1$),[2]

$$\mathcal{H}_{TB} = -t \sum_{\sigma} \sum_{\langle i,j \rangle} [a_\sigma^\dagger(\mathbf{R}_i) b_\sigma(\mathbf{R}_j) + \text{H.c.}], \tag{1}$$

where $a_\sigma(\mathbf{R}_i)$ $(b_\sigma(\mathbf{R}_i))$ annihilates and electron with spin $\sigma = \uparrow, \downarrow$ on sublattice $A(B)$ at position $\mathbf{R}_i$, and t (≈ 2.7 eV) is the nearest-neighbor hopping energy. When adatoms are added to graphene they can hybridize with an energy V to the C atoms and if the local Coulomb energy U is sufficiently large, a local moment of spin S is formed[8] at a site $\mathbf{R}_i$. This spin S_i interacts with the graphene electrons via an exchange interaction, $J_k \approx -V^2/U$, which is described by the Hamiltonian,

$$\mathcal{H}_s = J_k \sum_i S_i \cdot s_i, \qquad (2)$$

where s_i is the graphene electron spin. Equation (1) together with Eq. (2) describe a Kondo lattice in graphene.

Kondo interaction (2) induces an indirect kinetic exchange interaction between local moments, the RKKY interaction, which depends on the chemical potential μ and hence can be controlled with an external gate voltage. Therefore, the nature of the magnetic states in graphene can be controlled by the application of a transverse *electric* field, a situation that never occurs in metals. For low carrier concentrations, i.e., close to the Dirac point, the interaction between spins located in the same sublattice is ferromagnetic, $\chi_{AA}(\mathbf{R}) = \chi_{BB}(\mathbf{R}) \propto 1/R^3$, while it is antiferromagnetic if they belong to opposite sublattices ($\chi_{AB}(\mathbf{R}) \propto -1/R^3$).[14–17] Given the position of the magnetic moments and the effective interaction between them, we can perform numerical simulations to obtain the magnetic properties of the system.

When an adatom sits on top of a carbon atom, the carbon sp^2 bonds are locally distorted and acquire a sp^3 character as in diamond, with the carbon underneath the impurity being pulled out of the plane.[18] Although a flat graphene sheet has almost no magnetic anisotropy due to the very small spin-orbit coupling,[19] in the presence of ripples,[20] lattice distortions of the sp^3 type that are generated by the presence of adatoms such as H can substantially increase the spin-orbit interaction close to the adatoms, generating a local spin-orbit coupling up to $\Delta_{SO} \approx 7$ meV,[21] which corresponds to an out-of-plane magnetic anisotropy of ≈ 7 T. In the range of temperature $k_B T \lesssim \Delta_{SO}$, the minimal model for the interaction between adatoms in graphene should be correctly captured by the physics of the Ising model,

$$\mathcal{H}_{\text{eff}} = \sum_{i,j} J_{\text{RKKY}}(r_{ij}) S_i^z S_j^z - g\mu_B H_{ex} \sum_i S_i^z. \qquad (3)$$

where $J_{\text{RKKY}}(r_{ij})$ is a spatially dependent RKKY interaction that depends on μ and H_{ex} is an external magnetic field. For $\mu \ll t$, the period of the RKKY oscillation is long compared to the typical atomic distances and we only need to consider the power-law decay of the interaction. The exchange is given by $J_{AA}(r) = J_{BB}(r) = J_0 \exp(-r_{ij}/r_0)/r_{ij}^3$ for spins in the same sublattice and $J_{AB}(r) = -J_0 \exp(-r_{ij}/r_0)/r_{ij}^3$ for spins in different sublattices. r_{ij} is given in units of the lattice constant $a = 2.46$ Å and $r_0 \approx 12$ Å is a cutoff distance that is introduced to limit the range of the parameters in the numerical calculations.

III. RIPPLES AND ADSORPTION PROBABILITY

In a flat graphene layer, the magnetic interaction between impurity spins would generate uniform magnetic states. Nevertheless, ripples in the graphene structure break the translational symmetry and lead to an inhomogeneous situation where the adatoms have preferential sites for hybridization. Due to ripples, the topography of the surface in graphene is not flat but *has curvature, which appears* in the form of "valleys" and "hills." In graphene, the typical ratio between the height (h) and the lateral size (L) of the ripples is h/L

$\approx 0.1 - 0.2$.[5] On top of a hill, the characteristic curvature of the ripples distorts the sp^2 bonds to an extent that they acquire sp^3 character, with a significant hybridization between the σ and π bands. In this situation, the adsorption of a H atom on a hill C has been shown to be energetically favorable, helping to stabilize the ripple.[22] On the other hand, for perfectly flat graphene, the adsorption of a H atom costs some energy to locally distort the sp^2 bonds and pull the hydrogenated C atom out of the plane. The difference in the chemisorption energy between the two cases, recently calculated by *ab initio* methods, can be as large as 2.5 eV. These results also indicate the existence of a minimal curvature for the ripples ($h/L \gtrsim 0.12$) above which the adsorption of a H atom can be strongly favorable.[22] The substantial change in the chemisorption energy of H with the local curvature in graphene is qualitatively consistent with previous theoretical[23] and experimental[24] results in nanotubes, where the binding energy has been shown to change dramatically with the radius of the tube.

Assuming that graphene is supported on a substrate, only one surface is available for hybridization. Notice that because of curvature, the p_z orbitals that are locally perpendicular to the graphene surface, approach each other in the valleys but distance themselves in the hills. Contrary to the hill-C case, the local curvature is expected to inhibit the H adsorption in the valleys, since in order to stabilize the C-H bond relative to the other three C sp^3-like bonds, the H has to pull the C atom out of the plane against the curvature, at the expense of an additional cost of energy, compared to the flat case (the difference in chemisorption energies between the hill-C and the valley-C cases could easily amount to several eV). The H adatoms therefore hybridize much more easily in the hills than in the valleys, leading to a "percolative" structure as the planar density of adatoms is increased. Therefore, the probability that an adatom hybridizes with a hill C is larger than a valley-C atom.

Let us assume, for the sake of the argument, that the ripples in graphene have a simple sinusoidal form (see Ref. 5), that is, if z is the perpendicular coordinate of the C atom relative to the flat situation, then $z(x,y) = A \sin(k_x x + k_y y + \phi)$ where A, ϕ, k_x, and k_y are random parameters. A large number (up to 200) of such sinusoidal waves can be superimposed to obtain a randomly curved sheet, as shown in Fig. 1(a) for a system with $2 \times 600 \times 600$ C atoms. Next, we decide a strategy to allow the incorporation of adatoms by the graphene sheet for some quenched realization of ripples.

Given the existence of a lower bounded range of local curvature where the adsorption is most likely to happen,[22] and also the fact that the adsorption is much easier on the top of a hill rather than in the bottom of a valley in graphene, we assume a probability distribution that grows monotonically with the height of the ripples and has some effective lower cutoff, h_0, below which the adsorption is unlikely to happen. As a toy model, we may assume for instance that the probability of adsorption varies linearly with z through the following criterion: we allow the incorporation if

$$z > h_0 + h_i, \qquad (4)$$

where h_i is a random number varying from 0 to $z_{max} - h_0$, and $h_0 \in [-z_{max}, z_{max}]$ is the lower cutoff of the distribution, with
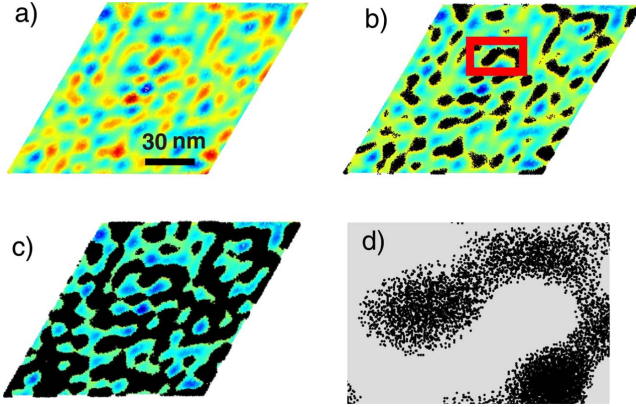
FIG. 1. (Color online) (a) Graphene sheet with random ripples. The color map represents the height increasing from blue to red in the interval $z \in [-z_{max}, z_{max}]$. (b) and (c) graphene sheet covered with adatoms for a lower cutoff $h_0 = 0.28 z_{max}$ and $h_0 = 0$ respectively (see main text). (d) Zoom in showing the adatoms on top of a hill (red rectangle).

z_{max} as the maximum height. The choice of another distribution function such as, for instance, a step function, $\theta(z - h_0)$, or some other distribution with a finite tail for $z < h_0$, should lead to similar conclusions regarding the physical properties, as far as the probability of adsorption on the top of the hills is large compared to the probability adsorption in the valleys.

If the number of atoms which are available for adsorption is fixed, by varying h_0 we obtain different incorporation fractions, as shown in Figs. 1(b) and 1(c). Notice that for a given realization of ripples, as one increases the adatom concentration, one obtains a percolative structure. At low coverage densities the adatoms form *clusters*. Hence, ripples naturally lead to clustering. We can also fix the total number of adatoms attached to the sample and see how the different probability functions change the coverage structure of the system. In this case, the overall structure is the same of Figs. 1(b) and 1(c) but different probability distributions lead to different concentrations of adatoms on top of the hills, as it will be clear in the next section.

IV. MAGNETIC TEXTURES

The details of the clustering depend on the nature of the adatoms used. For instance, if one uses H atoms, one might imagine that only H atoms that are separated by more than one lattice spacing are stable since H atoms which are in neighboring C sites can recombine into H_2 molecules and leave the graphene surface.[25] Hence, we have considered two different situations, namely, either the adatoms have nearest neighbors or not. We studied the location of magnetic adatoms using the same incorporation rules discussed above, with and without allowing the existence of nearest neighbors. For the system without first neighbors, we randomly remove the neighbors in order to avoid any artificial distribution of spins. We found that the magnetic response of these two systems are rather different and can be distinguished experimentally.

For a graphene sheet with full coverage, as shown in Fig. 2(a), we find that the moments order antiferromagnetically,
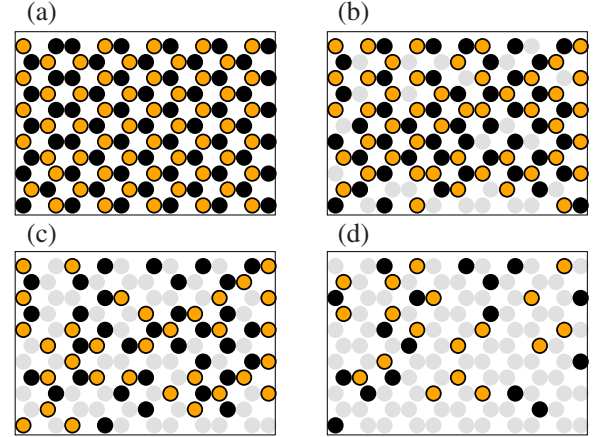

FIG. 2. (Color online) Spin configuration on top of a hill for (a) homogeneous coverage and (b)–(d) $h_0 = -1$, 0 and 0.28 z_{max} with adatom concentrations $x = 0.5$, 0.11, and 0.02, respectively. In black, spin up; in orange, spin down. ($k_B T = 0.01 J_0$).

as expected. Nevertheless, when we associate the local probability of adsorption of the adatoms to the ripples and we start to dilute the coverage for increasing values of h_0, the situation is rather more complicated. What we observe in Figs. 2(b)–2(d) is the destruction of the antiferromagnetic order on the clusters that are located on top of the ripples. The system becomes highly *frustrated* and finally for very low coverage we find that the system consists basically of weakly interacting isolated moments and clusters of few spins. One notices that the destruction of antiferromagnetic order is accompanied by a ferromagnetic tendency, that is, the clusters tend to *either remain antiferromagnetically ordered and interact ferromagnetically with nearest clusters* [see Fig. 2(c)] or order ferromagnetically in a situation that is reminiscent either of *superparamagnetism* or a *spin-glass* state.[26] In this paper we have considered only the average magnetic properties while disregarding rare events that can lead to Griffiths phases.[11] However, rare event physics can play an important role in these disordered magnetic systems and may contribute to the magnetic response. This is a problem, however, beyond the scope of the current manuscript.

For the configurations discussed above, we calculate the total average magnetization $M = M_A + M_B$ and the average staggered magnetization, $M_s = |M_A - M_B|$, in terms of the magnetization of each sublattice, M_A and M_B, as a function of the magnetic field H_{ex}. All the numerical simulations were performed for an Ising Hamiltonian with $2 \times 600 \times 600$ sites. We used 10 000 Monte Carlo steps for warm up and another 10 000 steps to collect the data. The magnetization is computed as an average over 160–400 realizations. As can be seen in Figs. 3(a) and 3(b) the maximally covered honeycomb lattice has always an antiferromagnetic correlation between the spins but as the coverage is reduced, this correlation is strongly suppressed, changing the shape of the hysteresis loops.

If we suppress the existence of nearest neighbors, one favors ferromagnetic interactions, once the interaction between next-nearest neighbors is ferromagnetic. However, as the magnetic atoms are randomly removed, we never pro-
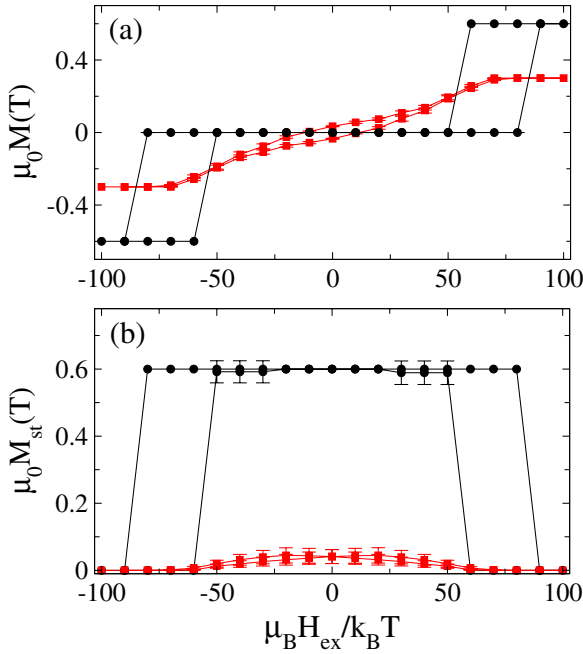
FIG. 3. (Color online) Left: (a) magnetization and (b) staggered magnetization as a function of an external magnetic field for a fully covered graphene sheet (black circles) and for $h_0=0$ (red squares) with $k_B T=0.01 J_0$.

duce a regular lattice of spins and do not have a perfect ferromagnetic system. Instead, for the system that was originally a regular honeycomb lattice, we see in Fig. 4(a) the formation of *magnetic domains* in the form of antiferromagnetically correlated *ferromagnetic stripes*. In the dilute situation [see Figs. 4(b)–4(d)] these ferromagnetic stripes are broken apart leaving behind ferromagnetic strings. The situation is clearly quite complex from the magnetic point of view and it is important to distinguish these various spin textures experimentally.
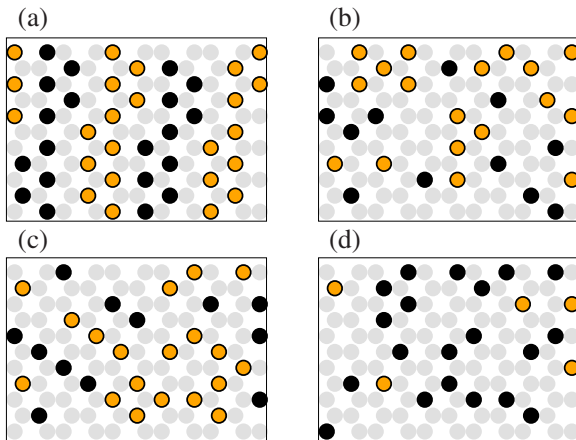

FIG. 4. (Color online) Spin configurations for the same hill considered in Fig. 2 but with the random removal of nearest neighbors. (a) homogeneous honeycomb lattice, and (b)–(d) $h_0=-1$, 0, and $0.28 z_{max}$, respectively. The adatom concentrations are (a) $x=0.24$ in the homogeneous lattice, (b) $x=0.22$, (c) $x=0.08$, and (d) $x=0.01$. In black, spin up; in orange, spin down ($k_B T=0.01 J_0$).
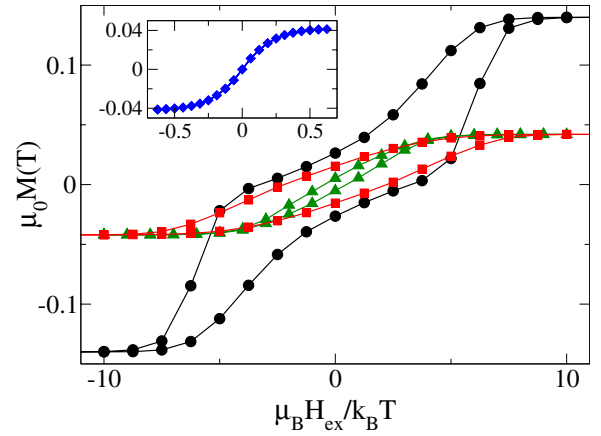

FIG. 5. (Color online) Magnetization as a function of magnetic field for a lattice without first neighbors: homogeneous lattice (black circles), $h_0=0$ and $k_B T=0.01 J_0$ (red squares) and $k_B T=0.05 J_0$ (green triangles). Inset: $h_0=0$ and $k_B T=0.2 J_0$ (blue diamonds).

In the case of an originally regular honeycomb lattice without neighboring adatoms, the magnetization $M(H)$ in Fig. 5 shows a large coercivity due to the ferromagnetic stripes (black circles), which decreases with smaller incorporation fractions. Whereas for large incorporation fractions we still can see the signature of antiferromagnetic correlations in the shape of the hysteresis curve, for smaller incorporation fractions the systems consists of ferromagnetic clusters with a typical ferromagnetic hysteresis loop (green triangles and red squares). By increasing temperature, we observe a decrease in the coercivity of the hysteresis loop. For $k_B T \gtrsim 0.2 J_0$ (see inset of Fig. 5), the spins interact weakly and we obtain a hysteresis loop that resembles a paramagnetic behavior. In this case, for low magnetic fields, H_{ex}, we find a universal linear dependence in the magnetization, $M \propto H_{ex}$.

It is important to point out the differences between the type of magnetic dilution we present here, compared to the usually magnetic diluted lattice, where the spins are randomly located, without any preferential position. In honeycomb lattices, randomly diluted spin systems have a site percolation transition at $p_c=0.697 04$.[27] For nearest-neighbor ferromagnetic interactions, the occurrence of a magnetic transition as a function of the dilution p has been shown to coincide with the percolation transition p_c.[28] For the antiferromagnetic case, recent results for the quantum Heisenberg Hamiltonian with site dilution[29] found that the magnetic long-range order persists above p_c. In any case, in the randomly diluted system the moments are always isolated and weakly coupled at very small concentrations ($p \ll p_c$). In this work, we have shown that due to the distribution of spins according to the structure of the ripples, we suggest the possible existence of strongly coupled magnetic clusters on top of the highest graphene hills, even at very low concentration of adatoms. Also, due to the ferromagnetic coupling between next-nearest neighbors, the moment of a given cluster will be bigger than zero even for a mostly antiferromagnetic one.

In Fig. 6, we compare the coverage structure and magnetization curves for three systems with the same adatom concentration, $x=0.05$, but different incorporation probability
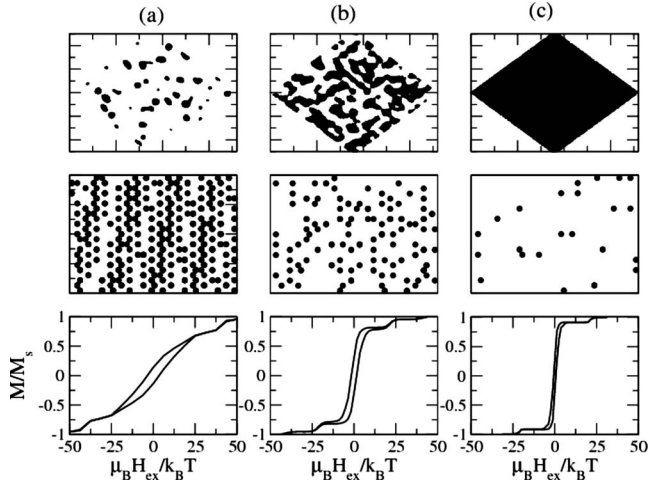
FIG. 6. The three columns show spin configurations (top), the details of the configuration for a small region of the system (middle) and total magnetization normalized by the value of saturation (M_s) versus magnetic field (bottom) for (a) $h_0=0.28z_{max}$, (b) $h_0=0$, and (c) a random distribution. The three systems contain the same concentration of adatoms, $x=0.05$.

distributions. The total concentration is the same in the three systems but h_0 sets regions where the presence of adatoms is forbidden. As a result, we can see the presence of strongly correlated clusters for $h_0=0.28z_{max}$, while for a random distribution of adatoms we found almost isolated spins. In addition, one can see the clear difference between the hysteresis loop in the correlated case (ripples), shown in Figs. 6(a) and 6(b), compared to the completely random one [Fig. 6(c)]. In the correlated case, we found regions with high concentration of spins and very strong antiferromagnetic correlations between them at low temperatures ($k_BT \ll J_0$), in contrast with the random case, where both hysteresis and the coercitive fields are very small.

V. MAGNETORESISTANCE

The interplay between the corrugated nature of graphene and its magnetic properties, which gives rise to the spin textures discussed above, can be probed by magnetotransport measurements. It was recently demonstrated that the incorporation of adatoms can dramatically change the transport properties in graphene,[13] where the system can go from a metallic behavior to a variable range hopping regime. In the case of magnetic impurities, due to the exchange interaction between the spin of the carriers and the adatom localized moments, the transport properties will be further modified by the interaction between spin and charge degrees of freedom. For strongly disordered graphene, which characterizes the regime of variable range hopping, the carriers are trapped with a binding energy E_i. Even at $H_{ex}=0$, the exchange interaction fully polarizes the localized spins interacting with a given localized carrier and increases its binding energy.[30]

If one considers the localized spins in the mean-field approximation, the exchange energy is given by $E_{ex}=J_k M_s \langle s \rangle$ where J_k is the exchange interaction between localized spins

and carriers, M_s is the saturation magnetization of the magnetic impurity spins and $\langle s \rangle$ is the mean value of the localized carriers spin. The total binding energy in the presence of the exchange interaction is given by $E_b=E_i+E_{ex}$ and has an associated Bohr radius ξ. It this situation, each spin is fully polarized in a random direction. If we apply an external field H_{ex}, the localized spins in the whole sample begin to align with the field and because of the exchange interaction between them and the band carriers, H_{ex} gives rise to a splitting of the conduction band. As a consequence, there is a *decrease* in the binding energy by $\Delta E_{ex}=J_k M(T,H)\langle s \rangle$. As $E_b \propto \xi^{-2}$, the magnetic field produces an increase in the effective Bohr radius

$$\xi_{eff}(T,H)=(E_i+J_k\langle s\rangle M_s[1-|M(T,H)|/M_s])^{-1/2}. \quad (5)$$

This effect is similar to the one observed in magnetically semiconductors as EuS or CdMnTe.[30]

The hopping probability between two states at a distance r is then given by $P=\exp(-2r/\xi_{eff}-W/k_BT)$ where W is the energy difference between the two states and ξ_{eff} is the characteristic Bohr radius of the localized states under the effect of an external magnetic field. Following the original Mott derivation, the resistance is[31]

$$\rho=\rho_0 \exp(T_0(H)/T)^{1/3}, \quad (6)$$

where

$$T_0(H) \propto 13.8/(k_B N(\mu)\xi_{eff}^2), \quad (7)$$

and $N(\mu)$ is the density of states at the Fermi energy. Since $T_0 \propto 1-|M(T,H)|/M_s$, we can extract the magnetoresistance curves of the system from our previous Monte Carlo results. In all curves, we normalize the scale of the magnetoresistance by the zero-field case, $R(H_{ex}=0)=1$. From the experimental point of view, the change in the temperature and gate voltage parameters in the range where Eq. (6) is applicable will additionally rescale the magnetoresistance curves. The scaling analysis of the magnetoresistance provides additional information allowing the empirical determination of the exchange interaction J_k and the binding energy E_i.

We begin our analysis by considering noninteracting spins. In this case, the response is paramagnetic and the magnetization curves follow a typical Brillouin function,

$$M(H_{ex},T) \propto \frac{2S+1}{2S}\coth\left(\frac{2S+1}{2S}x\right) - \frac{1}{2S}\coth\left(\frac{1}{2S}x\right) \quad (8)$$

where $x=g\mu_B S H_{ex}/k_B T$, and S is the spin quantum number. Assuming $g=2$ and $S=1/2$, we show in Fig. 7(a) the magnetoresistance curves for a system with noninteracting spins at different temperatures. The magnetoresistance is negative, reaching a minimum value when all the spins are aligned by the magnetic field. For a fixed magnetic field, the resistance grows with temperature.

Next, we present the magnetoresistance curves corresponding to the simulations in the previous sections. If we allow the presence of neighboring magnetic adatoms, the antiferromagnetic correlations between neighbors is strong and the minimum value of the magnetoresistance is only obtained for very large values of the magnetic field, set in en-
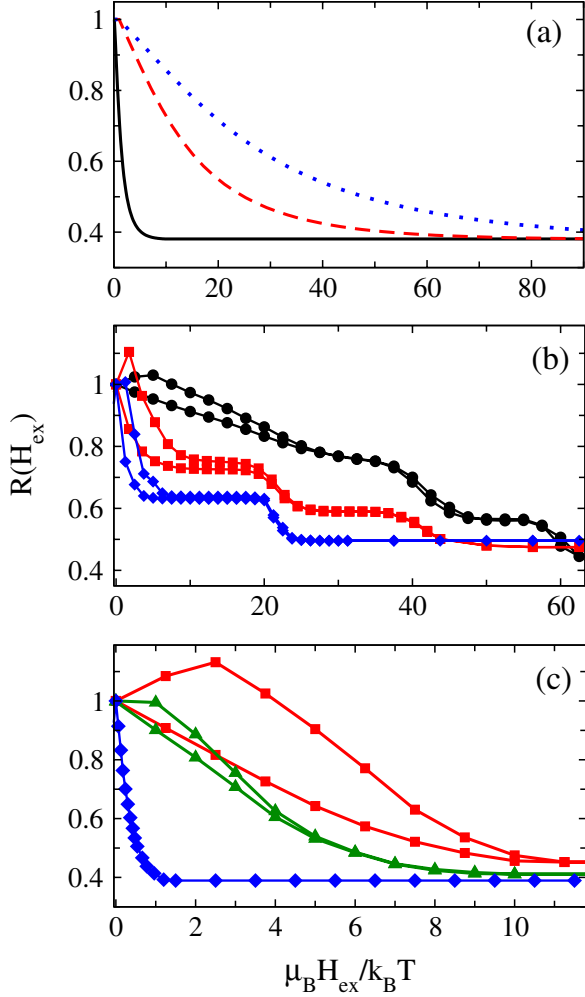
FIG. 7. (Color online) (a) Magnetoresistance for noninteracting spins at three different temperatures: $k_B T = 0.01 J_0$ (solid line), $k_B T = 0.1 J_0$ (dashed line), and $k_B T = 0.2 J_0$ (dotted line). (b) Magnetoresistance for the three different incorporation distributions shown in Fig. 6: $h_0 = 0.28 z_{max}$ (black circles), $h_0 = 0$ (red squares) and a random distribution (blue diamonds). (c) Magnetoresistance in the case without first neighbor H atoms for $h_0 = 0$ and different temperatures: $k_B T = 0.01 J_0$ (red squares), $k_B T = 0.05 J_0$ (green triangles), and $k_B T = 0.2 J_0$ (blue diamonds). All curves are normalized by the corresponding zero-field resistance $R(H_{ex} = 0) = 1$ and are symmetric for $H_{ex} < 0$.

ergy units of $k_B T$. In Fig. 7(b) we compare the magnetoresistance curves that correspond to the configurations shown in Fig. 6 for a fixed concentration of adatoms, $x = 0.05$, and different incorporation probabilities. In the correlated case [Figs. 6(a) and 6(b)] because of the fixed concentration of adatoms, the top of the highest ripples accumulates larger antiferromagnetic clusters for larger values of h_0, requiring the application of stronger magnetic fields to decrease the resistivity. On the other hand, for the case of random distribution of spins, the antiferromagnetic correlations are much weaker. Notice that for systems with hysteretic behavior in the magnetization, M is zero at the coercive field. Conse-

quently, the magnetoresistance at the coercive field is higher than its value for $H_{ex} = 0$, giving rise to a *positive* magnetoresistance at small fields.

In the scenario without nearest H neighbors, we consider the probability distribution with $h_0 = 0$, for different temperatures [see Fig. 7(c)]. For $k_B T \gtrsim 0.2 J_0$ the hysteretic nature of the magnetoresistance is considerably reduced and we obtain a curve that is similar to the case of noninteracting spins. Nevertheless, we note that the width of the resistivity peak is anomalously small, indicating that the effective size of such "noninteracting" moments is considerably larger than the moment of isolated adatoms. This is a clear indication for the presence of small magnetic clusters in graphene. For even higher temperatures, $k_B T \sim J_0$, the resistance decreases with H following $\rho \propto \exp(-\alpha H)$, where α is a constant that depends on the exchange interaction, density of states and temperature. For weak external fields $H_{ex} \ll \Delta_{SO}$, where Δ_{SO} is the spin-orbit coupling, the magnetoresistance will be strongly anisotropic and can vanish when the magnetic field is parallel to the graphene plane.

VI. CONCLUSIONS

In summary, we have discussed the possible magnetic states of magnetic adatoms on top of a rippled graphene sheet. We proposed the scenario where the nontrivial topography of graphene correlates the local moments of the adatoms, generating clusters and nontrivial macroscopic magnetic states. The magnetic order can be very sensitive to the value of the chemical potential, the adatom coverage, and the "repulsion" between adatoms for nearest-neighbor atoms.

We have found that while a perfectly covered graphene sheet has a strong tendency toward antiferromagnetism, the presence of ripples leads to more complex magnetic textures, with increased ferromagnetic tendency and even glassiness. We show that the hysteretic behavior of the magnetization provides a simple way to study these magnetic orderings. Nevertheless, the presence of different magnetic structures affects directly the transport properties. In the variable range hopping regime, the system presents a universal negative magnetoresistance that depending on the ratio between the exchange interaction, temperature and coverage fraction can have also show hysteretic behavior. The magnetotransport curves in graphene can provide clear experimental signatures for these nontrivial magnetic states.

[1] A. K. Geim and K. S. Novoselov, Nature Mater. **6**, 183 (2007).

[2] A. H. Castro Neto, F. Guinea, N. M. R. Peres, K. S. Novoselov, and A. K. Geim, Rev. Mod. Phys. **81**, 109 (2009).

[3] P. C. Hohenberg, Phys. Rev. **158**, 383 (1967); N. D. Mermin and H. Wagner, Phys. Rev. Lett. **17**, 1133 (1966).

[4] P. Chaikin and T. C. Lubensky, *Introduction to Condensed Matter Physics* (Cambridge University Press, Cambridge, 1995).

[5] J. C. Meyer, A. K. Geim, M. I. Katsnelson, K. S. Novoselov, T. J. Booth, and S. Roth, Nature (London) **446**, 60 (2007).

[6] E. Stolyarova, K. T. Rim, S. Ryu, J. Maultzsch, P. Kim, L. E. Brus, T. F. Heinz, M. S. Hybertsen, and George W. Flynn, Proc. Natl. Acad. Sci. U.S.A. **104**, 9209 (2007).

[7] N. M. R. Peres, F. Guinea, and A. H. Castro Neto, Phys. Rev. B **72**, 174406 (2005).

[8] B. Uchoa, V. N. Kotov, N. M. R. Peres, and A. H. Castro Neto, Phys. Rev. Lett. **101**, 026805 (2008).

[9] D. Withoff and E. Fradkin, Phys. Rev. Lett. **64**, 1835 (1990).

[10] K. Sengupta and G. Baskaran, Phys. Rev. B **77**, 045417 (2008).

[11] R. G. Griffiths, Phys. Rev. Lett. **23**, 17 (1969).

[12] A. H. Castro Neto and B. A. Jones, Phys. Rev. B **62**, 14975 (2000).

[13] D. C. Elias, R. R. Nair, T. M. G. Mohiuddin, S. V. Morozov, P. Blake, M. P. Halsall, A. C. Ferrari, D. W. Boukhvalov, M. I. Katsnelson, A. K. Geim, and K. S. Novoselov, Science **323**, 610 (2009).

[14] L. Brey, H. A. Fertig, and S. Das Sarma, Phys. Rev. Lett. **99**, 116802 (2007).

[15] V. V. Cheianov and V. I. Fal'ko, Phys. Rev. Lett. **97**, 226801 (2006).

[16] D. F. Kirwana, V. M. de Menezes, C. G. Rocha, A. T. Costa, R. B. Muniz, S. B. Fagan, and M. S. Ferreira, Carbon **47**, 2533 (2009).

[17] S. Saremi, Phys. Rev. B **76**, 184430 (2007).

[18] Y. Miura, H. Kasai, W. A. Dio, H. Nakanishi, and T. Sugimoto, J. Phys. Soc. Jpn. **72**, 995 (2003).

[19] H. Min, J. E. Hill, N. A. Sinitsyn, B. R. Sahu, Leonard Kleinman, and A. H. MacDonald, Phys. Rev. B **74**, 165310 (2006).

[20] D. Huertas-Hernando, F. Guinea, and A. Brataas, Phys. Rev. B **74**, 155426 (2006).

[21] A. H. Castro Neto and F. Guinea, Phys. Rev. Lett. **103**, 026804 (2009).

[22] D. Boukhvalov and M. Katsnelson, J. Phys. Chem. C **113**, 14176 (2009).

[23] O. Gulseren, T. Yildirim, and S. Ciraci, Phys. Rev. Lett. **87**, 116802 (2001).

[24] P. Ruffieux, O. Groning, M. Bielmann, P. Mauron, L. Schlapbach, and P. Groning, Phys. Rev. B **66**, 245416 (2002).

[25] J. S. Arellano, L. M. Molina, A. Rubio, and J. A. Alonso, J. Chem. Phys. **112**, 8114 (2000).

[26] J. A. Mydosh, *Spin Glasses* (Taylor & Francis, London, 1993).

[27] P. N. Suding and R. M. Ziff, Phys. Rev. E **60**, 275 (1999); X. Feng, Y. Deng, and H. W. J. Blote, *ibid.* **78**, 031136 (2008).

[28] A. R. McGurn, J. Phys. C **13**, 1055 (1980).

[29] E. V. Castro, N. M. R. Peres, K. S. D. Beach, and A. W. Sandvik, Phys. Rev. B **73**, 054422 (2006).

[30] T. Dietl, *Physics of High Magnetic Fields*, Springer Series in Solid State Science (Springer, New York, 1981), Vol. 24.

[31] N. F. Mott, Philos. Mag. **19**, 835 (1969).